PNAS RESEARCH ARTICLE | ENGINEERING

Flexible fluid-based encapsulation platform for water-sensitive materials

Baptiste Lemaire[a], Yanhao Yu[a], Nicola Molinari[a], Haichao Wu[a], Zachary A. H. Goodwin[a], Friedrich Stricker[a], Boris Kozinsky[a,1], and Joanna Aizenberg[a,b,1]

Contributed by Joanna Aizenberg; received May 25, 2023; accepted July 20, 2023; reviewed by Michael L. Klein and John A. Rogers

The next-generation semiconductors and devices, such as halide perovskites and flexible electronics, are extremely sensitive to water, thus demanding highly effective protection that not only seals out water in all forms (vapor, droplet, and ice), but simultaneously provides mechanical flexibility, durability, transparency, and self-cleaning. Although various solid-state encapsulation methods have been developed, no strategy is available that can fully meet all the above requirements. Here, we report a bioinspired liquid-based encapsulation strategy that offers protection from water without sacrificing the operational properties of the encapsulated materials. Using halide perovskite as a model system, we show that damage to the perovskite from exposure to water is drastically reduced when it is coated by a polymer matrix with infused hydrophobic oil. With a combination of experimental and simulation studies, we elucidated the fundamental transport mechanisms of ultralow water transmission rate that stem from the ability of the infused liquid to fill-in and reduce defects in the coating layer, thus eliminating the low-energy diffusion pathways, and to cause water molecules to diffuse as clusters, which act together as an excellent water permeation barrier. Importantly, the presence of the liquid, as the central component in this encapsulation method provides a unique possibility of reversing the water transport direction; therefore, the lifetime of enclosed water-sensitive materials could be significantly extended via replenishing the hydrophobic oils regularly. We show that the liquid encapsulation platform presented here has high potential in providing not only water protection of the functional device but also flexibility, optical transparency, and self-healing of the coating layer, which are critical for a variety of applications, such as in perovskite solar cells and bioelectronics.

water permeability | photoelectronic materials | device encapsulation | liquid-infused polymers

Significance

While water is essential to life, it is detrimental to semiconductors and electronics. However, the development of encapsulation methods to prevent the penetration of water has fallen behind the evolution of semiconductors and devices. Here, we report a bioinspired liquid encapsulation platform that not only protects water-sensitive materials from various water forms but also provides additional attractive features, including flexibility, transparency, self-cleaning, and self-healing. This technology is based on a polymer scaffold infused with a hydrophobic oil, whose exceptionally low water transmission is due to the small pore size of the scaffold and the low diffusion of water in the oil. The encapsulation layer is easily replenishable, resulting in long-term, renewable protection of the enclosed devices.

Water, in its various forms, can significantly reduce the performance and reliability of semiconductors and electronics, as the presence of water can lead to short-circuiting, corrosion, and degradation (1). Therefore, the prevention of water permeation at the material and device levels is essential for maintaining the operational stability of many state-of-the-art electronic, photonic, and energy systems. Currently, the main encapsulation methods to protect electronic devices from water damage are mechanical sealing and conformal coatings. Solid-state mechanical sealing is a hermetic encapsulation method that prevents moisture penetration (2) but increases device size and stiffness, making it incompatible with flexible electronics, and can lead to a mechanical failure with repeated usage. Conformal coatings are made with a polymeric film (e.g., epoxy resins, urethane, and silicone gels) (3), which are more flexible and compact, but they cannot provide absolute molecular-scale water protection over a long period of time, as the coating processes induce voids and cracks that break the seal, creating paths for water permeation.

The development of encapsulation methods has fallen behind the evolution of high-performance semiconductors and devices. For example, halide perovskites are a promising candidate for low-cost, high-efficiency thin-film solar cells because of their unique optoelectronic properties, including low binding energy of excitons, high carrier mobility, and long charge diffusion length (4, 5), but the intrinsically poor chemical stability and high sensitivity of anhydrous halide compounds to all types of polar molecules, in particular to water, prevent their industrial adoption (6–8). A wide range of solid encapsulation methods composed of glass, oxides, and polymers have been individually or jointly developed to protect perovskites (9–13). However, the current lifetime benchmark is still far behind the commercial requirement suggested by International Electrotechnical Commission (>10 y) (14). Moreover, emerging markets, such as optoelectronics and bioelectronics, simultaneously require high-level water protection together with one or more of the following properties: optical transparency, self-cleaning, and mechanical flexibility (15). For example, perovskite solar cells require optical transparency to convert solar energy into electricity and self-cleaning to prevent the accumulation of dust and other contaminants (11), while bioelectronic devices require

Author affiliations: [a]John A. Paulson School of Engineering and Applied Sciences, Harvard University, Cambridge, MA 02138; and [b]Department of Chemistry and Chemical Biology, Harvard University, Cambridge, MA 02138

Author contributions: B.K. and J.A. designed research; B.L., Y.Y., and N.M. performed research; F.S. contributed new reagents/analytic tools; B.L., Y.Y., N.M., H.W., Z.A.H.G., F.S., B.K., and J.A. analyzed data; and H.W., Z.A.H.G., B.K., and J.A. wrote the paper.

Reviewers: M.L.K., Temple University; and J.A.R., Northwestern University.

Competing interest statement: Patent application 0042697.00563WO1 filed on 30.10.2020.

[1]To whom correspondence may be addressed. Email: bkoz@seas.harvard.edu or jaiz@seas.harvard.edu.

This article contains supporting information online at https://www.pnas.org/lookup/suppl/doi:10.1073/pnas.2308804120/-/DCSupplemental.

Published August 14, 2023.

high mechanical flexibility to withstand stretching (16). Therefore, new encapsulation methods that combine high water repellency with flexibility, durability, temperature resistance, and optical transparency are still critically needed for the development and protection of next-generation devices.

In contrast to the current human-made encapsulations, living organisms have evolved various strategies to protect their highly sensitive chemical systems from the penetration of molecules and ions, including water. These strategies typically rely on viscous fluids and polymer networks that act in tandem to form a robust, flexible, self-replenishing coating. An excellent example is *Phyllomedusa sauvagii* (also known as waxy monkey tree frog), which in dry, hot seasons secretes an oily fluid that seals the channels and defects on its skin preventing the loss of water from the body. The frog periodically replenishes the wax and spreads it around its entire body, which allows the frog to survive without water for months (Fig. 1*A*) (17, 18). Similarly, inside the human body, mucus, a fluid-infused polymer matrix, protects the stomach lining by serving as a diffusion barrier against the harsh acidic environment (19), provides lubrication for efficient and smooth passage of food, self-heals upon perturbation, and can be replenished in response to acid level and food intake (20). The same general strategy of trapping liquids within the polymer matrix has been adapted in other parts of the body to combine diffusion control with mechanical compliance and self-cleaning (21, 22).

Inspired by these principles, we developed a conceptually similar encapsulation platform based on a hydrophobic oil-infused polymer matrix (Fig. 1*B*). The water protection characteristics of oil-infused polymer were tested with methylammonium lead iodide perovskite thin films ($MAPbI_3$) used as a proxy for extremely water-sensitive optoelectronic materials. The experimental results showed that the method of encapsulation with oil-filled polymer films can significantly reduce damage by water and extend the lifetime of the perovskite film. By combining the experiment with a comprehensive computational study, we provided a fundamental mechanism that accounts for the reduced water permeation: 1) inside the polymer matrix, with small pore sizes, the infused hydrophobic lubricant oil causes water to diffuse as clusters, and 2) the infused fluid also keeps the polymer matrix defect-free down to the molecular scale by infiltrating and self-eliminating artifact-induced and damage-induced low-energy diffusion pathways. We further demonstrated that the fluidic nature of the lubricant allows the system to be periodically purged of dissolved water molecules by replenishment of the oil overlayer that induces an outward diffusion of water from the matrix. In this way, the lubricant both within and on top of the material is kept "fresh," preventing the transition to the steady-state flow. Importantly, the polymer matrix infused with hydrophobic lubricant oil not only repels water droplets and moisture but also provides multiple functionalities, including optical transparency, pressure stability, self-cleaning, and self-healing.

Results

Liquid Encapsulation Platform. To test the hypothesis that our bioinspired strategy of oil incorporation (schematically shown in Fig. 1*B*) would improve the encapsulation quality of polymeric materials, we covered methylammonium lead iodide perovskite layer deposited on a fluorine-doped tin oxide (FTO)-coated glass substrate with a ~350-μm-thick Teflon® film, a commonly used hydrophobic membrane coating, and infused it with a high-viscosity perfluoropolyether lubricant, DuPont Krytox™ GPL 107 (density = 1.95 g/mL, kinematic viscosity = 1,600 cSt, dielectric constant = 2.1; note that the small dielectric constant means that the lubricant molecule is nonpolar and will not react with perovskites). Perovskites are extremely sensitive to water due to the strong affinity of methylammonium iodide (MAI) for water, leading to perovskite disassociation into PbI_2 and $MAI{\cdot}H_2O$. This disassociation results in a color change from dark brown to yellow, making the halide perovskite an ideal proxy for evaluating the encapsulation efficiency. The performance of oil-infused Teflon film was compared with that of uninfused, dry Teflon®-coated perovskite samples and bare perovskite exposed to water droplets (5 μL) on an inclined surface (Fig. 1*C*). The unprotected perovskite instantaneously decomposed upon contact with water. Being hydrophobic, the Teflon® film prevented the instantaneous degradation of perovskite, but the droplets pinned on the rough surface, allowing the water molecules to gradually permeate the membrane, and eventually decompose the perovskite after 6 min. In contrast, the lubricated surface shed the water droplets and the perovskite remained intact (Movie S1).

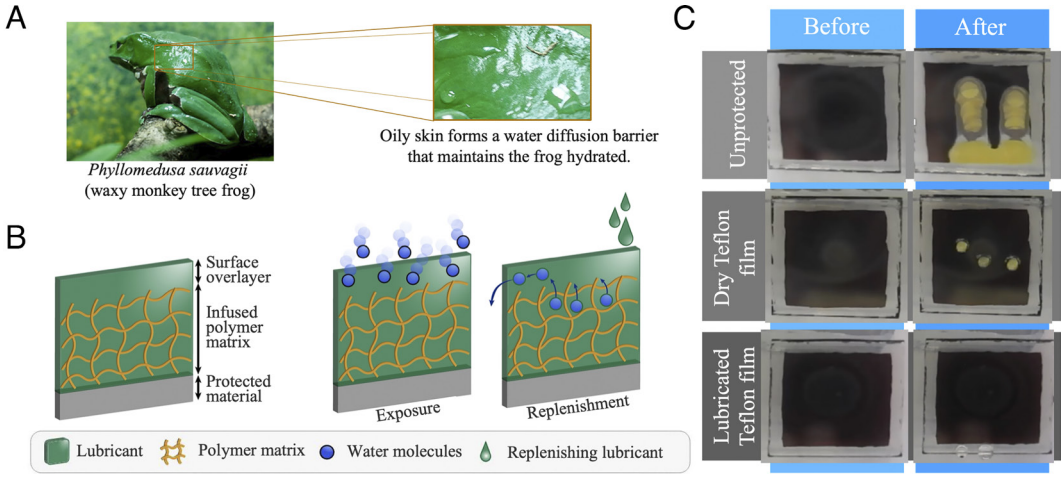

Fig. 1. Design features of the proposed liquid-infused polymer encapsulation approach. (*A*) Inspiration from the waxy monkey tree frog, an amphibian found in South America that secretes and periodically replenishes a protective oil to help its body retain moisture [Photo credits: Paul Hudson (23)]. (*B*) Schematic of the bioinspired working principle: a water-sensitive photoelectronic material is protected by a hydrophobic polymer scaffold infused with oil. After exposure to moisture or liquid water, the oil infusing the polymer can be periodically replenished to extend the protection. (*C*) Exposure of methylammonium lead iodide perovskite thin films to 5 μL water droplets on an inclined surface (30° from horizontal). From top to bottom: bare, protected with Teflon®, and protected with Krytox™ GPL K107-infused Teflon® membrane. The strong affinity of methylammonium iodide (MAI) to water leads to the perovskite degradation, which is detected by a change of color, from dark brown to yellow.

To systematically investigate the effects of chemical composition of the polymer matrix and infused lubricant oils on the stability of the protected perovskite films, we studied the water resistance of this liquid encapsulation system using fluoropolymer gels infused with fluorinated oils of various viscosities (Fig. 2*A*). In particular, we fabricated a range of fluoropolymer gels, or fluorogels, by polymerizing a perfluorinated alkyl acrylate monomer (2-perfluorooctylethyl acrylate, or PFOEA) with perfluoropolyether dimethacrylate (PFPE-DMA) in different volume ratios, based on previous work (24). The resulting fluorogels are chemically and thermally robust, transparent, with a mechanical behavior ranging from a soft elastomer (PFOEA—0 vol%) to a rigid plastic (PFOEA—100 vol%). Compared with Teflon® films, the fluorogel matrix is tough and stable, with pore sizes ranging from single digit to tens of nanometers (24). The oil-infused fluorogel, or lubrigel, is then obtained by infiltrating the elastomer with DuPont Krytox™ oils of different compositions and viscosities (dynamic viscosities ranged from ~20 to 3,000 cp, see *SI Appendix*, Table S1 for the complete characterization). Krytox™ lubricant oils are commonly used due to their high affinity to fluorinated elastomers, together forming stable and universally repellent (omniphobic) surfaces (25, 26). As both fluorogel and infused oils are based on highly fluorinated organic compounds, they are chemically inert to most substances and unlikely to interact with the protected water-sensitive materials. With an overcoated lubricant layer, the lubrigel (i.e., fluorogel infused with lubricant oils) displayed broad antifouling properties against water, hydrocarbon oils, proteins, and blood (24). Importantly for photoelectronic materials, both the dry fluorogel and the lubricant-infused gels are transparent to visible light. In addition, both fluorogel and Krytox™ lubricant oils are thermally stable up to 250 °C, thus temperature fluctuation for most application scenarios would not cause any degradation of the protective layer (24).

To evaluate the performance of these oil-infused fluorogel coatings (referred to as lubrigels) in comparison to unprotected and uninfused controls, we immersed the samples in a water bath (*SI Appendix*, Fig. S1). The dry fluorogel (~300 μm thick) protected the perovskite for ~20 h, while the unprotected perovskite film dissociated instantaneously (Fig. 2*B*). The Krytox™ K104-infused fluorogel stabilized the perovskite for more than 50 h in liquid water. Previous reports have indicated that a 1-h continuous immersion in water is roughly equivalent to ~90 h stability in the air (13). This suggests that lubrigel could provide over 4,500 h air stability. While we used a water bath for accelerated testing, we also demonstrated that both fluorogel and lubrigel encapsulation methods are able to protect perovskite from degradation for at least 4 mo in ambient air conditions (*SI Appendix*, Fig. S2).

The improved performance of the proposed lubrigel encapsulation, relative to dry fluorogel, brings a set of fundamental questions about the underlying water-protecting mechanism. The transmissibility of a gas through a membrane (vapor transport rate) is defined as $T = P/h$, where P represents the permeability and h represents the encapsulating film thickness. Therefore, the transmissibility decreases with the increase of the encapsulating film thickness, as shown in Fig. 2*C*. However, the observed stability cannot be explained by the effect of the increased thickness alone. In particular, when increasing the film thickness from 150 μm to 600 μm, the stability of perovskite protected by the dry fluorogel extended three-fold (from 11 ± 3 h to 34 ± 9 h), while the stability of perovskite protected by the lubrigel extended five-fold (from 19 ± 4 h to 100 ± 13 h). We hypothesized that this remarkable boost of the liquid encapsulation method was because the infused lubricant oil fills up the cracks and defects in the dry fluorogel, which are often unavoidable and provide potential pathways for water transport. To investigate this effect, we measured the topography in the polymer matrix via stationary laser scattering. The results showed that the defects in the polymer matrix are significantly reduced after the lubricant oil is infused into the dry fluorogel (*SI Appendix*, Fig. S3), indicating that oil infiltrates and removes cracks and defects in the membranes.

To analyze and optimize the performance of the lubrigel encapsulation barrier, we performed a comprehensive study exploring a broad range of copolymer ratios used in fluorogel synthesis and different polymer–lubricant combinations for perovskite samples immersed in a water bath. We observed a strong impact of the chemical composition of the polymer scaffolding on the encapsulation performance. For example, for K102-infused lubrigels, the stability of the perovskite thin films in a water bath extended nearly twofold

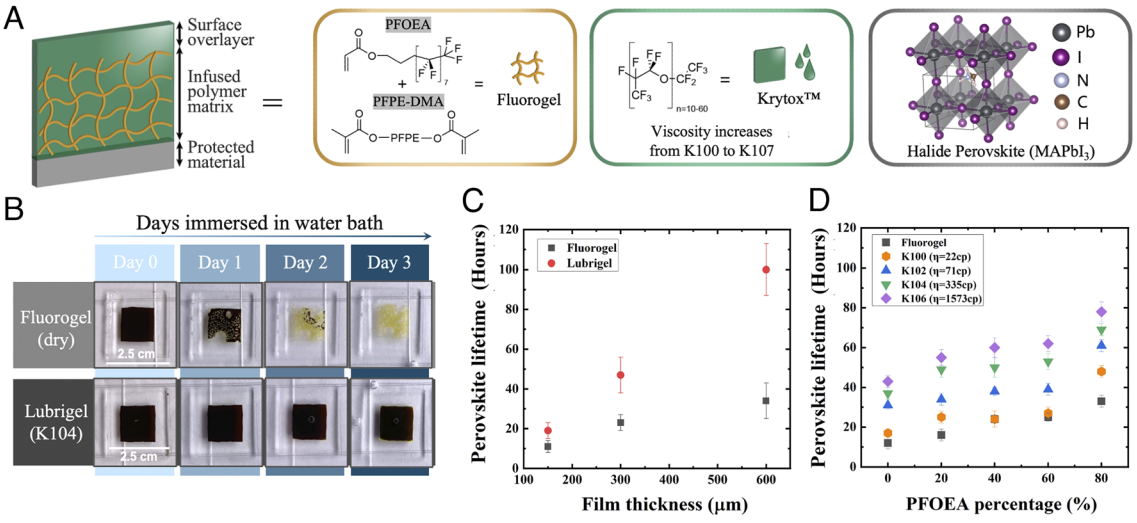

Fig. 2. Systematic study of the water-protective performance of an exemplary oil-infiltrated polymeric coating. (*A*) Components of the encapsulation system used in the current study. (*B*) The performance of a fluorogel (dry polymer matrix) and a lubrigel (fluorogel infused with Krytox™ K104) is compared by immersing the protected perovskite films in a water bath over the course of multiple days. (*C*) The lifetime of the perovskite thin films encapsulated by lubrigels (infused with Krytox™ K104) at 1:1 ratio of PFOEA:PFPE-DMA in a water bath as a function of the film thickness. Here, lifetime (stability time) is defined as the time it takes for perovskite films to change color from dark brown to yellow. (*D*) The lifetime of the perovskite thin films in a water bath as a function of different PFOEA:PFPE-DMA ratios, infused with different Krytox oils. Property details of various Krytox oils are summarized in *SI Appendix*, Table S1, lubrigel thickness is ~300 μm.

(from ~34 ± 3 h to ~61 ± 3 h) when the PFOEA percentage changed from 20 to 80 %. PFOEA contains more fluorinated groups than PFPE-DMA, which increases the hydrophobicity of the whole polymer matrix, so it is reasonable to expect a better water resistance with increasing of PFOEA percentage in the polymer matrix. The contact angle measurements that show a steady increase in the water contact angle with increased PFOEA concentration confirm this trend (*SI Appendix*, Fig. S4). In addition, PFOEA arranges itself in semicrystalline phases at the molecular level. This pronounced ordering results in a more compact and homogeneous polymer matrix with smaller pores (24), leading to an increase in stability when using fluorogels with higher PFOEA percentage. For the same reason, the Young's modulus of fluorogels increases by two orders of magnitude when PFOEA content increases from 20 to 100 % (*SI Appendix*, Table S2). In particular, the Young's modulus increases from 8 ± 0.8 MPa to 134 ± 22.8 MPa when increasing PFOEA from 60 to 80 %, which makes the polymer matrix significantly stiffer and thus unsuitable for encapsulating water-sensitive materials where flexibility is essential. Therefore, an optimal protective layer should be made of fluorogel with PFOEA:PFPE-DMA volume ratio around 4:6 to 6:4.

We further found that with increasing viscosity of the lubricant, the stability of perovskite thin film in a water bath is considerably increased, regardless of the composition of the polymer scaffolding used in the system (Fig. 2*D*). If the function of the infused oil is only to fill and eliminate the defects, as discussed above, then the increased viscosity should not have such a profound effect. We hypothesized that high-viscosity hydrophobic oils can inhibit the transport of water molecules. Given that the gradients of partial water pressure and the encapsulation layer thicknesses are comparable across experimental measurements, the origin of performance variation must arise from different permeabilities of water through the lubrigels. The permeability can be further expressed as $P = DS$, where D is the diffusion coefficient of water and S is the water solubility. All Krytox™ oils investigated demonstrated nearly identical water traces, as shown in *SI Appendix*, Fig. S5, which suggests that water solubility in these oils is nearly the same, and thus the diffusion coefficient must be responsible for the differences in performance.

Water Transport as Clusters of Water Molecules in Lubrigels. To understand the role of water diffusion, we performed atomistic molecular dynamics (MD) simulations of a representative system using LAMMPS (27). Each studied system was composed of 100 lubricant molecules (comprising 60 monomers of perfluoropolyether in a linear chain, unless otherwise stated), a single copolymer backbone with PFOEA:PFPE-DMA ratio of 1:1, and one or more water molecules. The OPLS-AA force field was utilized for the lubricant molecules and polymer backbone (28, 29), and the TIP4P force field was utilized for water (30). The full details of the calculation are described in the *Materials and Methods* section.

In the simulations, initially, the water molecules were dispersed and diffusing around independently. After some time, however, we found that the water molecules aggregate together and diffuse in a vehicular way. This is schematically shown in Fig. 3*A*. When there were 2 to 10 water molecules in the simulations, all of the water molecules would combine into a single cluster. However, when there were more than 10 water molecules in the simulation, they did not aggregate into a single cluster, but rather broke up into smaller clusters of up to 10 water molecules. Therefore, the water molecules in the lubrigel aggregate together into finite-sized clusters, instead of staying as free water molecules or bulk water.

To further understand the vehicular diffusion of water clusters, we computed the MSD of the water molecules, which is related to the diffusion coefficient, D, through MSD = $\langle [r(t) - r(0)]^2 \rangle$ = $6Dt$. The details of the calculation can be found in the *Materials and Methods* section. The MSD as a function of time for various water molecules in the simulation are shown in Fig. 3*B*. Clearly, a single water molecule has the largest MSD, with 2 water molecules having a smaller MSD, which further decreases for 4 and 10 water molecules. This reflects the fact that water molecules cluster together, diffusing as a single aggregate in a vehicular way, as schematically shown in Fig. 3*A* with the corresponding diffusion coefficients. From our experiments, we estimate a diffusion coefficient of ~10^{-12} m/s^2 from the time taken for degradation and device thickness, as detailed in the *Materials and Methods* section. This diffusion coefficient corresponds to 2 to 4 water molecules in a cluster from the simulations. From the Stokes–Einstein equation,

$$D = \frac{k_B T}{6\pi\eta R},$$

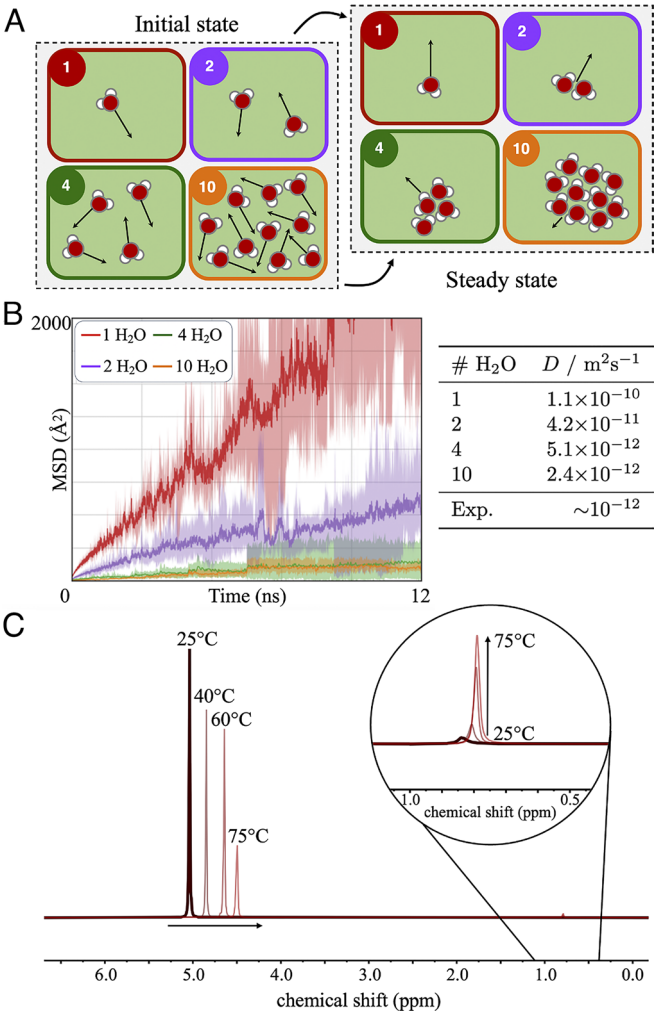

Fig. 3. Water clusters form in the lubrigel and slow down the diffusion of water molecules. (*A*) Schematic illustration of 1, 2, 4, and 10 isolated water molecules starting in the simulation, and the emerging steady-state regime of their clustered state. (*B*) Numerical data for mean squared displacement (MSD) computed for water molecules as a function of time, for various water clusters and single water molecules. Table on the right shows the computed diffusion coefficients from the MSD plots together with the measured experimental value. (*C*) Variable temperature ^{1}H-NMR (500 MHz, no solvent) of Krytox 106 with water at 25, 40, 60, and 75 °C. Two signals can be observed for water: the first signal corresponding to clustered water at around 5 ppm decreases and shifts upfield upon heating and the second signal corresponding to molecular water (see *Inset*) increases. This provides evidence for the presence of the water clusters in the oil-infused polymer that gradually break upon heating.

where η is the dynamic viscosity and R is the hydrodynamic radius of the diffusing species, the corresponding hydrodynamic radius is ~6 Å, which is significantly larger than the expected hydrodynamic radius of a single water molecule (1.6 Å from the TIP4P force field), indicating again that the water molecules tend to cluster together and diffuse in a vehicular way.

To verify this experimentally, we investigated the presence of water in hydrophobic Krytox™ oil using temperature-dependent ^{1}H-NMR. Upon addition of water to Krytox™ 106 lubricant oil at 25 °C, we observed two new signals: a large peak at 5.04 ppm and a small peak at 0.86 ppm (Fig. 3*C*). When the temperature was increased to 75 °C, the first peak shifted to 4.50 ppm while the second peak shifted to 0.79 ppm. Furthermore, the normalized integral of the signal at 0.86 increases from >0.01 to 0.04 upon heating to 75 °C. In line with other experimental investigation of water in hydrophobic oils (31, 32), the higher shift signal corresponds to the presence of water aggregates, while the low ppm signal results from the dissolved single water molecules. Upon heating, the aggregates are less stable and partially disassociate, leading to a shift in ppm toward dissolved single water molecules, and the peak corresponding to the dissolved water molecules increases significantly (see *Inset* in Fig. 3*C*). A comprehensive NMR measurement methodology and analysis are described in the *Materials and Methods* section, and *SI Appendix*, Figs. S6 and S7. Overall, the NMR results provide the experimental confirmation that a majority of water molecules form aggregates or clusters in the Krytox™ oil mixtures, which would slow down the rate of water transport through the coating.

Replenishment of Lubricant Oil Causes Back-Diffusion. To gain insight into the overall macroscopic mechanism for water transport, we solve the diffusion equation

$$\frac{\partial c}{\partial t} = D\frac{\partial^2 c}{\partial z^2},$$

where c is the concentration of water, based on the device geometry shown in Fig. 4*A*. Here, we assume that the lubricant overlayer has the same thickness as the lubrigel; the diffusion coefficient was the same in the lubricant film and polymer matrix; the concentration of water at the interface between the perovskite and polymer matrix is 0, as the water is assumed to immediately react with the perovskite on contact; and the water concentration at the contact between the water–lubricant overlayer interface is set by the solubility of water in the oil, c_0. Full details of the method used to solve the diffusion equation are shown in the *Materials and Methods* section.

Initially in the steady-state regime, as shown by t_0 in Fig. 4*A*, there is a linear concentration profile of water from c_0 to 0 across the device. Upon refreshing the lubricant, we instantaneously set the concentration of water to be 0 in the lubricant film, while leaving the concentration profile in the polymer matrix unaffected, as shown by the concentration profile t_1 in Fig. 4*A*. We then solve the diffusion equation based on this concentration profile, curves of which are given by t_2 and t_3, with $t_3 > t_2$. At the interface between the lubrigel and lubricant overlayer, we find that the water diffuses out of the polymer matrix, to increase the concentration of water in the lubricant overlayer. This causes the overall amount of water in the polymer matrix to decrease, but it also, eventually, decreases the gradient of the concentration profile at the perovskite–lubrigel interface, leading to the water vapor transmission rate (WVTR) toward perovskite, which is proportional to the concentration gradient, to decrease. Therefore, by refreshing the lubricant, back-diffusion of water out of the polymer matrix is initiated, which decreases the rate of degradation. Eventually, diffusion of water from the bulk causes back-diffusion to stop, and the polymer matrix is again filled with water until a steady state is reached again.

By refreshing the lubricant overlayer periodically, one can prevent the steady-state regime from ever being reached. The frequency of refreshment is a key parameter in the optimization of the encapsulation device. Refreshing the lubricant overlayer too frequently would protect the water-sensitive device but would waste a large volume of lubricant. On the other hand, not refreshing the lubricant overlayer frequently enough could damage the

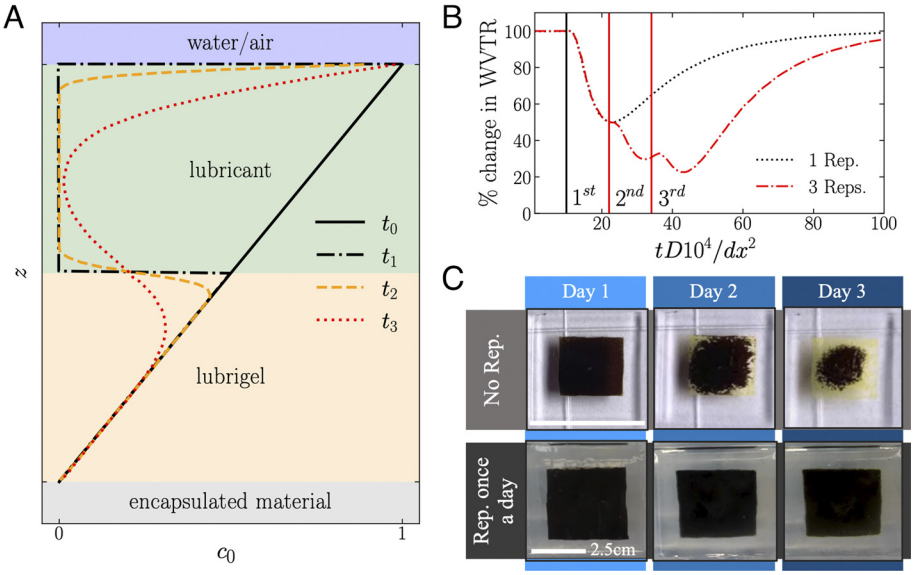

Fig. 4. Refreshing the lubricant overlayer causes back diffusion of water, further extending the lifetime of the encapsulated material. (*A*) Schematic of device geometry and computed concentration profiles at various stages in the refreshment cycle. (*B*) Numerical results showing the percentage change in water vapor transmission rate (WVTR), determined by the percentage change in the concentration gradient of water at the interface between the infused polymer matrix (lubrigel) and the encapsulated material. The data are shown for a single refreshment and three refreshing cycles. (*C*) Experimental data showing the effects of replenishment on the stability of the liquid encapsulation-protected perovskite thin film.

device by allowing water time to diffuse to the interface. Therefore, there exists an optimal refresh rate that should substantially extend the lifetime of the perovskite. In Fig. 4*B*, we show an example of refreshing the lubricant overlayer 1 time and 3 times. The WVTR, expressed in percentage change, is reduced and extended over larger timescales.

Inspired by the numerical results, we investigated the effects of replenishment experimentally and found that the lifetime of the perovskite thin film considerably increased by replenishing the lubricant oil every day. For example, the perovskite thin film protected by PFOEA-50 infused with K102 oil began to degrade on day 2, while replenishing the lubricant oil every day ensures full stability on day 3 and beyond, as shown in Fig. 4*C*. These experimental results further confirm the simulation prediction that replenishing lubricant oil will lead to back-diffusion of water and extend the longevity of the protected perovskite thin film.

Other Functional Properties. In addition to the exceptional water repellency, this liquid encapsulation platform also provides high flexibility, surface slipperiness, self-healing, and transparency—characteristics which are critically important for the functionality of emerging electronics, but which the traditional encapsulation methods cannot satisfy.

Mechanical properties. Adapting our technology to stretchable systems requires the encapsulating materials to have a relatively low Young's modulus. The fluoropolymer has an elastic modulus ranging from a few MPa to ~350 MPa depending on the PFOEA: PFPE-DMA ratio (*SI Appendix*, Table S2). In particular, a fluorogel with 60 vol% PFOEA is soft and easily stretchable, with an elastic modulus of about 8 MPa, yet provides excellent stability in water. To assess the performance of the lubrigel encapsulation under mechanical stress, we prepared lubrigel-over-perovskite samples deposited on a flexible polyethylene terephthalate (PET) substrate. We immersed the two samples bent in opposite directions in a water bath (*SI Appendix*, Fig. S8). Both samples remained intact for more than 2 d in water, suggesting that the lubrigel could provide more than 4,500 h stability in air even under large mechanical deformation.

Optical properties. The encapsulation must be transparent for visible light when used as protection for optoelectronics. Importantly, not only the polymer matrix and lubricant themselves are transparent but previous work also shows that an atomically smooth lubricant overlayer present on the polymer surface can further enhance optical transparency (33). We confirmed this observation by measuring the UV-visible light transmittance in the incoming wavelength range of 300 to 800 nm (*SI Appendix*, Fig. S9). For perovskite protection, in addition to transparency, an ideal encapsulating layer should be able to reflect or absorb UV, as long-time UV exposure can irreversibly damage the perovskite (14). Here, our transmittance measurements show that the fluorogel and lubrigel absorb or reflect more in the UV range than glass while being more transparent in the rest of the visible spectrum (>98% for both gels, as opposed to about 90% for glass), making it an ideal encapsulation technology for UV-sensitive optoelectronics.

Surface slipperiness and self-cleaning. Surface slipperiness markedly increases the repellency of encapsulations to impinging water droplets and ice (34, 35). We quantified the slipperiness by measuring the contact angle hysteresis of water droplets using a goniometer (*SI Appendix*, Fig. S10). Even after multiple days of immersion in water, the lubrigel maintains a very low contact angle hysteresis, providing the coating with self-cleaning properties, when dust and other surface contaminants are easily removed by a moving water droplet.

Self-healing. The mobility of the lubricant within and over the polymer ensures the self-healing property of the lubrigel coatings, as the defects are easily filled by the directional diffusion of infused oils from the bulk to the affected site (24, 36, 37), which helps maintain excellent water resistance even when the surface is physically damaged (Movie S3).

Discussion

The liquid encapsulation platform we have presented displays an ultralow water transport rate to prevent water infiltration while providing customizable wetting, mechanical, and optical properties. Using halide perovskite as a model system because of its ability to change color upon dissolution, we demonstrated that water damage is drastically reduced when the sensitive layer is protected by a hydrophobic polymeric matrix filled with a matching hydrophobic oil. While this work mainly focused on understanding the fundamental water transport mechanisms, our further research aims to apply this platform to a detailed study of the device performance characteristics and degradation of function in situ.

We note that the choice of a fluoropolymer gel and fluorinated lubricants in this work was dictated by the following reasons: as we show, the PFOEA-PFPE copolymer can be synthesized in different volume ratios of the components, and thus, its physicochemical properties can be easily tunable. The resulting fluorogels were, therefore, excellent candidates for our fundamental study, since we could comprehensively describe the water diffusion characteristics as a function of 1) the mechanical properties of the polymer (from a soft elastomer to a rigid plastic); 2) its crystallinity; 3) the pore sizes of the network available for lubricant incorporation; 4) polymer hydrophobicity; and 5) lubricant molecular weight and viscosity. It is important to emphasize, however, that the concept of a liquid encapsulation platform is not limited to fluorogels and fluorinated lubricant oils, whose potential may be influenced by the regulations of per- or polyfluorinated alkyl substances (PFAS) due to environmental effects (38, 39). The presented principle could be extended to various hydrophobic polymer matrices, such as acrylic, poly(vinyl chloride) polymers, or silicone gels, as long as they work as conventional conformal coatings, combined with an infused hydrophobic oil, such as silicone, mineral, or vegetable oil, that is compatible with the supporting polymer network and does not react with the protected, water-sensitive materials. This makes the proposed platform amenable for environmentally friendly real-world applications, including the protection of various complex three-dimensional devices as the fluidic property of the lubrigel makes it possible to coat and infuse the entire shape via dip coating (40).

From a fundamental mechanistic perspective, we established general design guidelines for creating multifunctional water-impermeable coatings for emerging semiconducting materials and devices. Through tuning the dynamics of lubricant constraint, vapor diffusion, and replenishment, we can optimize this liquid encapsulation platform for different applications. In particular, using both experiments and simulation, we systematically investigated the effects of polymer scaffolding and lubricant oil on the stability of perovskite films, elucidating the basic transport mechanisms of water diffusion in the complex polymer matrix/infused oil environment. We found that water tends to aggregate into water clusters, which are extremely sensitive to the polymer network pore size and the lubricant viscosity, leading to an ultralow water transmission rate. (We note that the elevation of temperature will increase the diffusion coefficient of water molecules based on Stokes–Einstein equation, which will cause a slight decrease in water resistance and the associated reduced longevity.)

Furthermore, similar to the frog's ability to secrete and replenish the wax on its surface, a key advantage of the developed encapsulation device is the potential to refresh the oil overlayer, effectively removing all the water from this overlayer. We argue that this important property is due to the unique regeneration mechanism involving the reversal of the diffusion direction of water clusters. Such a reversed concentration gradient leads to water diffusion away from the water-sensitive components, extending the longevity of the protected materials. We believe that the routine replenishment of hydrophobic oils in solar cell farm scenarios, for example, could be possible if integrated with regular maintenance of solar cells, and the replenishment frequency could be accurately predicted based on the diffusion model demonstrated here.

In summary, the liquid encapsulation platform provides a new strategy to address the long-standing challenge of water protection, suggesting opportunities in a variety of applications, such as perovskite solar cells and bioelectronics. In addition to the exceptional water protection performance, this approach also offers other attractive properties, including optical transparency, high flexibility, and self-healing—critical characteristics, which are impossible to achieve simultaneously for traditional hermetic encapsulation methods. Importantly, this design principle can be readily applied to other fluid–polymer hybrids, and, more broadly, can open up an exciting path to controlling the molecular transport properties of soft materials.

Materials and Methods

Materials. The perfluorinated PFPE GPL lubricants (DuPont Krytox™ 100-107) used for fluoropolymer infusion were purchased from Miller-Stephenson. Teflon® membranes with an average pore size of 200 nm and a thickness of about 350 μm were purchased from Sterlitech Corporation, WA, USA and used as received without further modification. Methylammonium iodide (anhydrous), lead(II) iodide (perovskite grade), N, N-dimethylformamide (anhydrous, 99.8%), and FTO-coated glass slides, purchased from Sigma-Aldrich, and 2-propanol (anhydrous, 99.5%), purchased from Beantown Chemical, were all used as received.

Fabrication of Methylammonium Lead Iodide Perovskite Thin Films. $CH_3NH_3PbI_3$ perovskite thin films were prepared via spin coating (41). First, 30 wt% lead(II) iodide (perovskite grade) in N, N-dimethylformamide (anhydrous, 99.8%) was spin-coated onto FTO–coated glass substrates at 6,000 rpm for 40 s. After the thus prepared PbI_2 layer fully dried, 10 mg/mL methylammonium iodide (CH_3NH_3I or MAI) solution in 2-propanol was spin-coated onto it at 6,000 rpm for 40 s and then annealed at 150 °C for 1 min. These MAI spin-coating and annealing steps were repeated three times. The excess MAI was washed away using 2-propanol, affording the final product as a dark-colored $MAPbI_3$ perovskite thin film.

Fabrication of Krytox™ Oil-Infused Fluorogel. The fluorogel was fabricated by mixing 2-perfluorooctylethyl acrylate (PFOEA) and Fomblin MD-40 (PFPE-DMA, 4 kg/mol) at various volume ratios with 3 vol% of photoinitiator (Darocur 1173) and then curing the mixture under UV light for 3 min under nitrogen atmosphere (24). The infusion with the DuPont Krytox™ PFPE GPL lubricants (100–107) into the as-prepared fluorogel was performed to form Krytox™ oil-infused fluorogel (lubrigel). The excess oil can be removed by using a spin coater, and the thickness of the remaining oil overlayer is directly related to the spin speed and time. A thin overlayer of oil was generally left on the surface to ensure that the lubrigel has antifouling and self-cleaning properties.

Measurements of Perovskite Thin Films Stability in a Water Bath. To evaluate the effects of polymer matrix composition and infused oil viscosity on protecting perovskite thin films from degradation in water, we fully immersed the prepared encapsulated perovskite thin films in a water bath at ambient conditions (*SI Appendix*, Fig. S1). The stability time was recorded when the color change of protected perovskite thin film (i.e., from dark brown to yellow) was observed. Note that 1-h continuous immersion in water is roughly equal to ~90 h stability in the humid air, according to previous literature (13).

Measurements of the Macroscopic Diffusion Coefficient of Water. The macroscopic diffusion coefficients of water in the encapsulating materials were approximated by using $D = L^2/t$, where L represents the characteristic length (thickness of encapsulated layer) and t represents the experimental measured stability time. For example, when L equals to 300 μm and the measured stability time is 10 h, the diffusion coefficient is $\sim 2.5 \times 10^{-12} m^2/s$.

Solubility Measurements. Mixed solutions of Krytox and water (volume ratio of about 1:1) were prepared and vigorously stirred at 40 °C for 1 wk. The solubility measurements were then conducted using the Deluxe Digital Water Test Kit from Sandy Brae Laboratories and following the standard procedure for the range A [0 to 1,500 ppm], leading to a resolution of 1 ppm and an accuracy of ±15 ppm.

Contact Angle and Hysteresis Measurements. Contact angle measurements were performed using a goniometer (CAM 101, KSV instruments) under ambient conditions. Deionized water was used as a probing liquid for both contact angle and contact angle hysteresis measurements. Contact angles were measured for 5 to 10 μL droplets.

NMR Measurements. Variable temperature ^{1}H-NMR spectra were recorded using Varian I500 NMR Spectrometer operated at 500 MHz without a solvent. All measurements were referenced of tetramethylsilane (TMS), with the Krytox Oil signal at 5.96 serving as a reference for all measurements without TMS.

Transparency Measurements. UV–Vis–NIR transparency measurements were performed using a Cary 7000 Universal Measurement Spectrophotometer. We measured the transparency in the 200 to 1,600 nm domain.

Mechanical Measurements. Mechanical properties of various fluorogels were measured using a tensile tester (Instron 5965, Instron Co.). Dumbbell-shaped fluorogel thin films (width 2 mm, length of 10 mm, thickness ~0.2 mm) were measured at a tensile velocity of 1 mm/min. Young's modulus was determined as the slope from the stress–strain curve at strains ranging from 0 to 0.25 depending on the sample.

Molecular Dynamics Simulations. The initial configurations of our MD simulations were created using the Materials Science module of the Schrodinger software suite (42). Each system was composed of 100 lubricant molecules (comprising 60 monomers of perfluoropolyether in a linear chain, unless otherwise stated), a copolymer backbone with PFOEA:PFPE-DMA ratio 1:1, and one or more water molecules in periodic boundary conditions. To run MD simulations, we used LAMMPS (27) and the OPLS-AA force field (28), directly given by the Materials Science program, for the lubricant molecules and polymer backbone. The TIP4P force field (30), with long-range Coulombic Solver (Particle-Particle Particle-Mesh) (43), was used for water. As the water angle and bonds are constrained in the TIP4P force field, a timestep of 2 fs was utilized. The temperature was controlled using a Nose–Hoover thermostat in an isothermal-isobaric ensemble (NPT) at 300 K and 1 atm to match the conditions of our experiments. To enhance the sampling of the phase space and to compute averages and SDs, we performed every calculation on an ensemble of 10 independently generated structures.

We calculated the MSD of water molecules. At a fixed temperature, MSD gives us access to the diffusion coefficient via the following expression:

$$D = \frac{1}{6N}\frac{d}{dt}\sum_i^N \left[r_i(t) - r_i(0)\right]^2 = \frac{1}{6}\frac{d}{dt}\mathrm{MSD}(t),$$

where N is the number of water molecules averaged over. The MSD calculations were computed over 12 ns.

Finite Element Simulations. We used a forward time-centered space numerical scheme to solve the diffusion equation in 1D:

$$\frac{\partial c(x,t)}{\partial t} = D\frac{\partial^2 c(x,t)}{\partial x^2} = \frac{c_i^{n+1} - c_i^n}{\Delta t} = D\frac{c_{i+1}^n - 2c_i^n + c_{i-1}^n}{\Delta x^2},$$

where c_i is the concentration of water at the spatial gridpoint I and the temporal gridpoint n, D is the overall diffusion coefficient of water, Δt is the timestep size, and Δx is the spatial stepsize. This is a well-developed Euler method for solving the diffusion equation. This method is conditionally stable, and we cautiously kept our parameters (spatial and temporal stepsizes) within the domain of stability, $\frac{D\Delta t}{\Delta x^2} \leq \frac{1}{2}$.

We assumed that the concentration at the water–lubricant interface is the maximum concentration at saturation c_0 and that the water at the interface between the encapsulation layer and the protected material reacts immediately with the water-sensitive layer. Therefore, the concentration at the interface of the encapsulated material can be approximated to 0. We further assumed that the diffusion coefficient is identical in the lubricant overlayer and in the lubricant-infused polymer matrix, and that there is no barrier to diffusion at the interface between these two. Upon refreshing the lubricant overlayer, the concentration of water inside the lubricant overlayer was set to zero, apart from that at the water–lubricant boundary where it was enforced to be c_0, and at the boundary between the lubricant and polymer, it was momentarily set to the concentration it had in the previous time step. The WVTR was determined from the concentration gradient at the interface of the encapsulated material. We calculated it in terms of percentage change relative to the steady-state regime.

Data, Materials, and Software Availability. All study data are included in the article and/or supporting information.

ACKNOWLEDGMENTS. This work is supported by the NSF through the Designing Materials to Revolutionize and Engineer our Future program under Award No. DMR-1922321 and the Harvard University Materials Research Science and Engineering Center under Award No. DMR-2011754. Note that portions of this work are part of the PhD dissertation of Dr. Baptiste Lemaire.

1. I. Baylakoğlu *et al.*, The detrimental effects of water on electronic devices. *e-Prime Adv. Electr. Eng. Electron. Energy* **1**, 100016 (2021).
2. S. Emami, J. Martins, D. Ivanou, A. Mendes, Advanced hermetic encapsulation of perovskite solar cells: The route to commercialization. *J. Mater. Chem. A* **8**, 2654–2662 (2020).
3. J. Wu, R. T. Pike, C. P. Wong, N. P. Kim, M. H. Tanielian, Evaluation and characterization of reliable non-hermetic conformal coatings for microelectromechanical system (MEMS) device encapsulation. *IEEE Trans. Compon. Packaging Manuf. Technol.* **23**, 721–728 (2000).
4. M. Gratzel, The light and shade of perovskite solar cells. *Nat. Mater.* **13**, 838–842 (2014).
5. A. K. Jena, A. Kulkarni, T. Miyasaka, Halide perovskite photovoltaics: Background, status, and future prospects. *Chem. Rev.* **119**, 3036–3103 (2019).
6. S. Cheng, H. Zhong, What happens when halide perovskites meet with water? *J. Phys. Chem. Lett.* **13**, 2281–2290 (2022).
7. Y. Rong *et al.*, Challenges for commercializing perovskite solar cells. *Science* **361**, eaat8235 (2018).
8. Y. Wang *et al.*, Encapsulation and stability testing of perovskite solar cells for real life applications. *ACS Mater. Au* **2**, 215–236 (2022).
9. Y. Zhao *et al.*, A polymer scaffold for self-healing perovskite solar cells. *Nat. Commun.* **7**, 10228 (2016).
10. S. Ma *et al.*, Development of encapsulation strategies towards the commercialization of perovskite solar cells. *Energy Environ. Sci.* **15**, 13–55 (2022).
11. Y. Shi, F. Zhang, Advances in encapsulations for perovskite solar cells: from materials to applications. *Solar RRL* **7**, 2201123 (2023).
12. Y. Zhan, J. Peng, C. Cao, Q. Cheng, A biomineralization-inspired strategy of self-encapsulation for perovskite solar cells. *Nano Energy* **101**, 107575 (2022).
13. F. Bella *et al.*, Improving efficiency and stability of perovskite solar cells with photocurable fluoropolymers. *Science* **354**, 203–206 (2016).
14. C. C. Boyd, R. Cheacharoen, T. Leijtens, M. D. McGehee, Understanding degradation mechanisms and improving stability of perovskite photovoltaics. *Chem. Rev.* **119**, 3418–3451 (2019).
15. Q. Shen *et al.*, Liquid metal-based soft, hermetic, and wireless-communicable seals for stretchable systems. *Science* **379**, 488–493 (2023).
16. Z. Zhang *et al.*, High-brightness all-polymer stretchable LED with charge-trapping dilution. *Nature* **603**, 624–630 (2022).
17. L. A. Blaylock, R. Ruibal, K. Platt-Aloia, Skin structure and wiping behavior of phyllomedusine frogs. *Copeia* **1976**, 283–295 (1976).
18. BBC (Frog applies 'sun cream'–Natural World: Attenborough's Fabulous Frogs - BBC Two). https://www.youtube.com/watch?v=z16ndVyJGBQ.
19. L. Laine, K. Takeuchi, A. Tarnawski, Gastric mucosal defense and cytoprotection: Bench to bedside. *Gastroenterology* **135**, 41–60 (2008).
20. B. Button *et al.*, A periciliary brush promotes the lung health by separating the mucus layer from airway epithelia. *Science* **337**, 937–941 (2012).
21. S. W. Chang, I. L. Tsai, F. R. Hu, L. L. Lin, Y. F. Shih, The cornea in young myopic adults. *Br. J. Ophthalmol.* **85**, 916–920 (2001).
22. M. E. Johansson, H. Sjovall, G. C. Hansson, The gastrointestinal mucus system in health and disease. *Nat. Rev. Gastroenterol. Hepatol.* **10**, 352–361 (2013).
23. P. Hudson, Giant Waxy Monkey Tree Frog (2011), https://www.flickr.com/photos/pahudson/5514017464/.
24. X. Yao *et al.*, Fluorogel elastomers with tunable transparency, elasticity, shape-memory, and antifouling properties. *Angew. Chem. Int. Ed Engl.* **53**, 4418–4422 (2014).
25. X. Yao *et al.*, Adaptive fluid-infused porous films with tunable transparency and wettability. *Nat. Mater.* **12**, 529–534 (2013).
26. T.-S. Wong *et al.*, Bioinspired self-repairing slippery surfaces with pressure-stable omniphobicity. *Nature* **477**, 443–447 (2011).
27. A. P. Thompson *et al.*, LAMMPS–A flexible simulation tool for particle-based materials modeling at the atomic, meso, and continuum scales. *Comput. Phys. Commun.* **271**, 108171 (2022).
28. W. L. Jorgensen, J. Tirado-Rives, The OPLS [optimized potentials for liquid simulations] potential functions for proteins, energy minimizations for crystals of cyclic peptides and crambin. *J. Am. Chem. Soc.* **110**, 1657–1666 (1988).
29. W. L. Jorgensen, D. S. Maxwell, J. Tirado-Rives, Development and testing of the OPLS all-atom force field on conformational energetics and properties of organic liquids. *J. Am. Chem. Soc.* **118**, 11225–11236 (1996).
30. W. L. Jorgensen, J. Chandrasekhar, J. D. Madura, R. W. Impey, M. L. Klein, Comparison of simple potential functions for simulating liquid water. *J. Chem. Phys.* **79**, 926–935 (1983).
31. K. Oka *et al.*, Long-lived water clusters in hydrophobic solvents investigated by standard NMR techniques. *Sci. Rep.* **9**, 223 (2019).
32. M. P. Conrad, H. L. Strauss, The vibrational spectrum of water in liquid alkanes. *Biophys. J.* **48**, 117–124 (1985).
33. S. Sunny *et al.*, Transparent antifouling material for improved operative field visibility in endoscopy. *Proc. Natl. Acad. Sci. U.S.A.* **113**, 11676–11681 (2016).
34. P. Kim *et al.*, Liquid-infused nanostructured surfaces with extreme anti-ice and anti-frost performance. *ACS Nano* **6**, 6569–6577 (2012).
35. P. W. Wilson *et al.*, Inhibition of ice nucleation by slippery liquid-infused porous surfaces (SLIPS). *Phys. Chem. Chem. Phys.* **15**, 581–585 (2013).
36. S. Kolle *et al.*, On the mechanism of marine fouling-prevention performance of oil-containing silicone elastomers. *Sci. Rep.* **12**, 11799 (2022).
37. N. Vogel, R. A. Belisle, B. Hatton, T. S. Wong, J. Aizenberg, Transparency and damage tolerance of patternable omniphobic lubricated surfaces based on inverse colloidal monolayers. *Nat. Commun.* **4**, 2176 (2013).
38. T. N. Penland *et al.*, Trophodynamics of per- and polyfluoroalkyl substances in the food web of a large Atlantic Slope River. *Environ. Sci. Technol.* **54**, 6800–6811 (2020).
39. G. Fauconier, T. Groffen, V. Wepener, L. Bervoets, Perfluorinated compounds in the aquatic food chains of two subtropical estuaries. *Sci. Total Environ.* **719**, 135047 (2020).
40. P. Le Floch *et al.*, Wearable and washable conductors for active textiles. *ACS Appl. Mater Interfaces* **9**, 25542–25552 (2017).
41. Y. Kutes *et al.*, Direct observation of ferroelectric domains in solution-processed CH3NH3PbI3 perovskite thin films. *J. Phys. Chem. Lett.* **5**, 3335–3339 (2014).
42. Materials Science Suite, Schrödinger, LLC: New York, https://www.schrodinger.com/platform/materials-science.
43. R. W. Hockney, *Computer Simulation Using Particles*, J. W. Eastwood, J. W. Eastwood, Eds. (McGraw-Hill International Book Co., New York, 1981).